Modeling the lava heat flux during severe effusive volcanic eruption an important impact on surface air quality

Jonathan Durand, Pierre Tulet, Maud Leriche, Soline Bielli, Nicolas Villeneuve, Andrea Di Muro, Jean-Baptiste Fillipi

To cite this version:

Jonathan Durand, Pierre Tulet, Maud Leriche, Soline Bielli, Nicolas Villeneuve, et al.. Modeling the lava heat flux during severe effusive volcanic eruption an important impact on surface air quality. Journal of Geophysical Research: Atmospheres, 2014, pp.119. 10.1002/2014JD022034 . hal-01164000

JOURNAL OF GEOPHYSICAL RESEARCH, VOL. ???, XXXX, DOI:10.1029/,

Modeling the lava heat flux during severe effusive volcanic eruption: an important impact on surface air quality

Jonathan Durand,[1] Pierre Tulet,[1] Maud Leriche,[2] Soline Bielli,[1] Nicolas Villeneuve,[3] Andrea Di Muro,[3] and Jean-Baptiste Fillipi[4]

---

[1] LACy, UMR 8105, CNRS - Université de La Réunion, Météo-France

[2] LA, UMR 5560, CNRS - Université de Toulouse III

[3] IPGP, UMR 7154, CNRS - Université Paris Diderot

[4] SPE, UMR 6134, CNRS - Université de Corse

Abstract. The Reunion Island experienced its biggest eruption of Piton de la Fournaise volcano during April 2007. Known as “the eruption of the century”, this event degassed more than 230 KT of SO_2. Theses emissions led to important health issues, accompanied by environmental and infrastructure degradations. This modeling study uses the mesoscale chemical model MesoNH-C to simulate the transport of gazeous SO_2 between April 2nd and 7th, with a focus on the influence of heat fluxes from lava. This study required the implementation of a reduced chemical scheme, a basic surface model and an estimation of lava heat fluxes in the atmospheric model. The model was able to reproduce general trends of this eruption, in particular the crossing of trade wind inversion, the SO_2 surface concentration (with highest peak of SO_2 of 600 $\mu g\ m^{-3}$ observed April 4th for western Reunion locations), and the wet deposition associated to rainfall. A sensitivity study shows that without heat fluxes over the vent and the lava flow, simulated SO_2 surface concentration are up to 45 times higher than observed.

1. Introduction

1.1. Generalities

Volcanoes are one of the most important natural sources of air pollution, both during and between eruptions [*Oppenheimer*, 2003]. It is essential for different areas of atmospheric science to have a good knowledge of volcanic volatile emissions in time and space, their atmospheric chemistry, physical and radiative effects. There are two different types of volcanoes: "reds" volcanoes characterized by relatively quiet effusive eruptions and transmitting any fluid lava in the form of castings, and “gray” volcanoes characterized by explosive eruptions and emitting pasty lava and ash in the form of pyroclastic flows. Each type of volcano is impacting the atmosphere in very different way, particularly in terms of injection depth and nature of the products ejected. Explosive volcanic eruptions such as those of El Chichon (Mexico) in 1982 [*Pollack et al.*, 1983; *Hoffman*, 1987] and Mount Pinatubo in 1991 [*McCornick et al.*, 1995; *Fiocco et al.*, 1996; *Robock*, 2002], mainly affected climate because of radiative and chemical impact of the plumes formed by aerosols injected into the stratosphere [*Solomon*, 1999; *Robock*, 2000, 2002]. For effusive volcanic eruptions such as those of Piton de la Fournaise (Reunion Island, Indian Ocean), the problem is different. Knowledge of their atmospheric and environmental impacts in the troposphere and degassing processes has some shortcomings. By chemical oxidation reactions, volcanic gases such as SO_2, which is predominant during the degassing of the lava, become acidic and can interact with the aerosol phase as precursors of particles through nucleation and/or condensation. These tropospheric volcanic aerosols play an important role in atmospheric radiation, directly by scattering and absorbing of short wave radiation, and indirectly by changing cloud cover and cloud properties [*Hobbs et al.*, 1982; *Al-*

brecht, 1989; *Kaufman et al.*, 2000; *Yuan et al.*, 2011a, b]. Tropospheric volcanic aerosols and gaseous compounds, especially sulfur dioxide, can also be source of risks to terrestrial ecosystems and health at local or regional scales [*Baxter et al.*, 1982; *Mannino et al.*, 1996; *Allen et al.*, 2000; *Delmelle et al.*, 2001]. Piton de la Fournaise is a typical basaltic shield volcano located on the Indian Ocean Island of Réunion and, as Etna and Kilauea, it is one of the world's most active effusive volcanoes, with an eruption occurring every 10 months in average [*Roult et al.*, 2012]. Reunion island is born 3 million years ago in the emergence of a gigantic volcano, in the southwest of the Indian Ocean at 21.06°S and 55.32°E. It presents on its 2512 km² a unique variety of landforms and landscapes with Piton des Neiges (3071m) being its highest point. The orographic influence on local dynamics of Reunion Island expected to be major. The interaction of the high mountainous terrain with the synoptic flow induces a large variability of wind field at local scale. The maritime and tropical location of the island, as well as the complexity of the terrain and wind exposure, imply a multitude of local circulations and weather, marked by large variations in temperature and precipitation. Modeling of local circulations is very complex to achieve in an environment like Réunion Island because it is the result of a complex interaction between topographic circulations, thermal breezes and local formation of clouds and precipitation. During an eruption, other parameters make modeling more difficult, including the effects of the dynamics of volcanic flows and thermal secondary effects associated with lava flow. Few studies, as the Vog Measurement and Prediction Project (VMAP) on island of Hawaii (http://mkwc.ifa.hawaii.edu/vmap/hysplit), have been able to accurately represent the distribution of volcanic pollution at characteristic scales of a volcanic island. The Piton de la Fournaise eruption of April 2007 presented all the characteristics of complex flow of sulfur dioxide with a temporal discontinuity between the highest concentrations of surface SO_2

observed and the paroxysmal period of emission from the vent. The sulfur dioxide SO_2 is the second gas emitted at the Piton de la Fournaise volcano after water H_2O, followed by carbon dioxide CO_2 and hydrochloric acid HCl. The objectives in the framework of this case study are two-folds. First the paper aims to investigate the complex transport and distribution of the sulfur dioxide influenced by steep topography and three-dimensional atmospheric circulation. The second objective is to highlight the influence of the cloud scavenging and the heat fluxes on the SO_2 surface concentration. For the latter, high resolution numerical simulations have been used to analyze the sensitivity of the heat fluxes on the volcanic pollutants. This paper starts with a brief description of April 2007 eruption as well as numerical methods (section 2). Section 3 is devoted to analyzing the estimation of the heat flux release during the eruption. The section emphasizes the influence of lava flow on the convection and its consequences on the SO_2 distribution.

1.2. Description of the April 2007 eruption of the Piton de la Fournaise

In April 2007, the Reunion's Island has known its biggest eruption of Piton de la Fournaise volcano at least three centuries [*Michon et al.*, 2013]. Within a month, 210 Mm^3 of lava flowed out with 90 Mm^3 reaching the sea. Above all, the collapse of the summit caldera caused significant morphological change [*Michon et al.*, 2007]. Due to this nearby events and large environmental and civil protection impacts, this eruption is very well described in literature [*Staudacher et al.*, 2009; *Vlastélic et al.*, 2012; *Barde-Cabusson et al.*, 2011; *Tulet and Villeneuve*, 2010; *Di Muro et al.*, 2014]. After two short eruptive events (18 February and 30 March), a critical phase of the eruption started at 06 UTC on 2 April, located on the lower south-eastern part of the volcano (55°46" 25.5' E ; 21°16" 54.6' S ,WGS84) at only 590m above the sea level and only 3km from the coast (Figure 1). In less than eleven hours, two main lava streams reached the sea, producing significant water vapor plumes with a very low pH due to strong presence of sulfuric and chlorohydric compound (pH<2 , *Staudacher et al.* [2009]). During the first two day, lava fountains up between 50m and 150m high were observed. From 4 April, MODIS sensor shows a significant increase of the lava flow rate until the 6th of April, where the peak of emissions of lava was observed (greater than 200 m^3/s at the vent, *Coppola et al.* [2009]; *Staudacher et al.* [2009]). SO_2 emissions, proportional to lava emissions, were estimated at 80 kg s^{-1} the 4 April 12 UTC, 320 kg s^{-1} the 5 April 12 UTC and 1600 kg s^{-1} the 6 April 12 UTC before a strong decrease until 8 April 12 UTC at 55 kg s^{-1}, and finally a constant emission of 55-70 kg s^{-1} until 11 April [*Tulet and Villeneuve*, 2010]. The peak of degassing was simulated at 1800 kg s^{-1} on April 6, with the total budget estimated at 230kT, which is in agreement with the petrologic estimation of 311kT [*Di Muro et al.*, 2014]. The Observatoire Volcanologique du Piton de la Fournaise (OVPF) recorded the 5 April at 20:48 UTC an earthquake of 4.8 magnitude synchronous with the caldeira collapse [*Michon et al.*, 2007; *Staudacher et al.*, 2009]. As described in *Tulet and Villeneuve* [2010] the location of this ash plume is well separate from the SO_2 one, as well as the vapor plume. The 6 April, lava fountains reached more than 200m high, and there were several tens of individual lava flows from 2 to 20m wide [*Staudacher et al.*, 2009]. At this moment, the lava flow reaches its maximum lateral and longitudinal extents. In late 6 April, the intensity dramatically decreases, and the eruption became more “typical” compared to usual eruptions of Piton de la Fournaise. The 12th of April, the shallow seismicity came back at its highest , causing a new Dolomieu crater collapse. In the next days, the lava eruption intensity became steady with effusion measured at 15-20 $m^3.s^{-1}$. This last event continued until May 1st 2007, the last eruption day.

1.3. ORA observations

ORA (Observatoire Réunionnais de l'air) provides daily monitoring of air pollution levels. It is equipped with several fixed and mobile stations along the Reunion coastline, measuring continuously primary and secondary pollutants. During the April 2007 eruption, 8 stations measured the SO_2 surface concentration from Saint Louis to Saint Denis passing through Cambaie in the west (Figure 1). Data from these three stations are compared to simulations. The first day, surface concentration of SO_2 is very low with value under 20 $\mu g\ m^{-3}$ for all stations (Figure 2). The next day from 02 UTC, Saint Louis and Cambaie stations measured significant increases of SO_2 concentrations with a peak of more than 60 $\mu g\ m^{-3}$ for Cambaie and 200 $\mu g\ m^{-3}$ for Saint Louis at 06 UTC. The 4th of April, new strong increases of surface concentration have been measured by all stations located on the southwest and northwest coast. A peak of 600 $\mu g\ m^{-3}$ was observed at Cambaie and 587 $\mu g\ m^{-3}$ in Saint Louis at 13 UTC. A significant decrease followed this peak of SO_2 surface concentration, with SO_2 concentration falling below the 100 $\mu g\ m^{-3}$ threshold at the end of the day. The 5th, a slight increase appears at dawn (from 03 UTC) with 200 $\mu g\ m^{-3}$ for Cambaie and 269 $\mu g\ m^{-3}$ for Saint Louis. Subsequently, from the 5th (12 UTC) to the 10th of April (06 UTC), the concentration varied between 20 $\mu g\ m^{-3}$ to 120 $\mu g\ m^{-3}$ for all west coast station except Saint Louis station, where brief peaks appeared for few hours on the 10th (345 $\mu g\ m^{-3}$) and the 24th (390 $\mu g\ m^{-3}$) . The highest values measured by ORA are not in phases in time with the maximum emitted from the vent. This paradox needs a detailed study of sulfur dioxide transport.

2. Model description

2.1. Atmospheric model

The mesoscale non hydrostatic atmospheric model (MesoNH) developed by the Centre National de la Recherche Météorologique and the Laboratoire d'Aérologie [*Lafore et al.*, 1998] has been used for the study. MesoNH can be used at all scales ranging from synoptic to large eddy scales (http://mesonh.aero.obs-mip.fr/). It can be run in a two way nested mode involving up to eight nesting stages. Different sets of parameterizations have been introduced for convection [*Bechtold et al.*, 2001; *Pergaud et al.*, 2009], cloud microphysics [*Cohard and Pinty*, 2000], turbulence [*Bougeault and Lacarrere*, 1989], lightning [*Barthe et al.*, 2007], gaseous chemistry [*Suhre et al.*, 1998; *Tulet et al.*, 2003], cloud chemistry [*Leriche et al.*, 2000] and aerosols [*Tulet et al.*, 2005; *Grini et al.*, 2006].

2.2. Surface model

The SURFEx surface scheme is coupled with MesoNH to simulate surface processes, thermodynamic and chemical exchanges with the atmosphere. (http://www.cnrm.meteo.fr/surfex/; Masson et al, 2013.). SURFEx is composed by various parameterizations for natural land surface [*Noilhan and Mahfouf*, 1996; *Bougeault and Lacarrere*, 1989], urbanized area [*Masson*, 2000], lakes and oceans [*Salgado and Le Moigne*, 2010] and chemistry and aerosols surface processes [*Tulet et al.*, 2003; *Mokhtari et al.*, 2012]. The coupling with the atmospheric model is performed by averaging the surface fluxes over a model grid box. Within SURFEx, the lava flow is represented by a line of potential heat flux emission, starting from the vent of the volcano at 21.28°S and 55.77°E to the coastline at 21.28°S and 55.80°E. This representation implies two major approximations for the lava flow. The first one is the misrepresentation of lava flow shape, as the observed lava flow has a triangular shape. The second is relative to the static representation of the lava under SURFEx, when the lava propagation is not integrated in time. The increasing surface of lava flow and its heat flux is modeled by multiplying the line of potential emission with a coefficient proportional to the increase of the lava flow surface.

2.3. Model configuration

The simulation starts at 00 UTC on April 2nd 2007, and ends at 00 UTC on April 7th 2007. The simulation has two nested domains with Kessler microphysics scheme and TKE turbulence scheme (prognostic turbulent kinetic energy, one and a half order closure). The largest domain with high model grid spacing (2km) is centered over the Reunion island. The domain extends over 330km from north to south and 450km from east to west. The second domain covers only the Reunion Island and its coastline with a horizontal model grid spacing of 500m. The vertical grid is composed of 72 levels for both models stretching up to 31km altitude with a first level 5m above ground level. Initial and lateral boundary conditions are extracted from ECMWF analysis for the meteorological fields and from MOCAGE (http://www.cnrm.meteo.fr/gmgec/spip.php?article87) for gaseous chemistry fields. The gas phase chemistry is resolved on both domains using the ReLACS chemical mechanism [*Crassier et al.*, 2009], which is a reduced version of RACM including the oxidation of sulfur dioxide by OH radical. In SURFEX, the entire SO_2 emission is released at the vent. This assumption is well correlated with the fact that the magma begin to degas when it reaches the vent and its surroundings. In consequence, with a 500m MesoNH horizontal model grid spacing, the location of SO_2 emission is well represented. A simulation protocol was implemented to limit the model drift by reinitializing the model dynamic (wind, humidity and temperature filed) in the middle of the simulation while the chemical fields have been preserved along the whole period (Figure 3). A second simulation starts the 3rd at 18 UTC until the 4th of April at 00 UTC. This latter provides at its end the dynamic fields refresh, while suppressing the need for model spin-up (time taken by the model to reach equilibrium state). Finally, a new simulation starts the 4 April at 00 UTC with the dynamic of simulation 2 and chemistry of simulation 1.

Sensitivity tests are made in this study to highlight the influence of heat fluxes in the transport of volcanic pollutants and the influence of cloud chemistry in scavenging sulfur dioxide. The 3 simulations configurations are sum up in the table 1.

3. Estimations of thermodynamic emissions

3.1. Heat flow estimation

Lava heat is released in the atmosphere from the core of an active flow by conduction through the basal, lateral and surface crusts [*Oppenheimer*, 1991; *Klingelhofer et al.*, 1999; *Quareni et al.*, 2004]. At the surface, heat losses are dominated by radiation (5×10^4 W m^{-2}) and convection (10^4 W m^{-2}), whereas conduction from the base to the ground is predominant (10^3 W m^{-2}, *Harris et al.* [2005]). For this study, only convective heat fluxes are implemented, with the assumption that heat losses by conduction and by rain falling on the flow (250 W m^{-2}, *Harris et al.* [2005]) are negligible. As the influence of radiant heat fluxes is inversely proportional to the square of the distance; we have also neglected it for our simulation. The heat flow by convection is calculated from:

$$Q_{conv} = hc(T_{surf} - T_{air})$$

With *hc* the heat transfert coefficient estimated at 50 W m^{-2} by *Keszthelyi et al.* [2003], T_{surf} the lava surface temperature and T_{air} the air temperature (290K). Estimation of the sensible heat fluxes, and hence the lava cooling, is mainly controlled by the surface winds. The heat flux relation to the wind from Keszthelyi observations are taken into account in our model (Figure

4). The surface covered by hot (1100°C) liquid lava flow and the crusted (400°C) lava is taken from the day by day observation given by *Bachèlery et al.* [2014] between April 2nd and 8th, allowing the estimation of the heat flow (in m^2) from the ground.

4. Sulfur transport during the April 2007 eruption of Piton de la Fournaise volcano using MesoNH atmospheric model

4.1. SO_2 mass burden

Figure 5 represents the evolution of SO_2 mass burden simulated by MesoNH between April 3rd and April 6th at 18 UTC. The first period until 4 April shows that the plume is oriented to the west with a maximum of mass burden of 210 DU. From April 5 and 6, the plume at the vent, above 5km ASL is oriented to the north with a large value (330 DU) over Reunion island. During this period, the strong presence of SO_2 in the north of Reunion Island indicates a plume separation. The change in direction between the two periods is due to the SO_2 plume crossing the inversion of trade winds around 3500m-4500m ASL. Below the inversion, a lower branch of the SO_2 plume is transported westward by the trade winds, while above, an upper plume is advected eastward. This analysis of SO_2 plume evolution in the first 4 days of the eruption is consistent with the study based on satellite data OMI and CALIOP by Tulet and Villeneuve (2010).

4.2. Simulated SO_2 surface concentrations

In the morning of April 2, the SO_2 plume at the surface is oriented southwestwards, contourning by the south the Piton de la Fournaise area. The plume is then transported along the coastline influenced by the trade winds circumventing the island, where a strong gradient of SO_2 appears. During this day, the SO_2 plume reaches Cambaie, at the northwest of the island with low surface concentration of SO_2 in order of some tens of $\mu g\ m^{-3}$. The strongest simulated concentrations are located at low altitude, near Saint Joseph in the south, with 350 $\mu g\ m^{-3}$. For other stations, SO_2 surface concentration is 125 $\mu g\ m^{-3}$ at Saint Louis in the southwest or a comparatively low 25 $\mu g\ m^{-3}$ is observed in Sainte Thérèse in the northwest, while concentrations in Saint Denis to the north is even lower with 1 $\mu g\ m^{-3}$. Not much changes occur the 3th of April, when the overall atmospheric dynamics confine the volcanic pollutants to the west of the island (Figure 6, dots represent ORA stations, Saint Denis at the north, Cambaie at the northwest and Saint-Louis at the southwest). Concentrations for the majority of the stations are stronger than the eve, with 200 $\mu g\ m^{-3}$ at Saint Louis and 75 $\mu g\ m^{-3}$ at Cambaie and Sainte Thérèse (Figure 6). However, the strong SO_2 gradient noted earlier is no longer present on April 3rd. SO_2 distribution appears larger on the south and west side of La Reunion and to the west above the ocean.

Higher concentrations are simulated the 4th of April, with a peak of 680 $\mu g\ m^{-3}$ obtained at St. Joseph and 350 $\mu g\ m^{-3}$ obtained at St. Louis. For stations in the north of the island, the concentrations are close to of those April 3rd. The maximum SO_2 concentration at the surface is thus located in the heights of the island, where high concentrations are simulated notably with more 1000 $\mu g\ m^{-3}$ in the heights above the city of Saint Joseph (south of Réunion Island). On the 5th of April, an increase of heat flow and a decrease in the stability of the atmospheric boundary layer allows the plume to reach higher altitude and in consequence be oriented directly to the northwest.

Finally, the 6 April, high concentrations are only simulated over the entire southern half of the island, with concentrations over 5000 $\mu g\ m^{-3}$, 10 times the threshold recommended by European standards. Unfortunately, no observations are available in the south of the island to validate these very high-simulated concentrations the 6 April.

4.3. Comparison between MesoNH simulation and ORA data

From 2 to 5 April, the simulation succeeds to correctly reproduce general trends for all simulated stations on the island (Figure 7). On the 2nd, the SO_2 surface concentration given by MesoNH corresponds to ORA observations for these three stations with values below 15 $\mu g\ m^{-3}$ for Cambaie and Saint Denis and a peak of 200 $\mu g\ m^{-3}$ in the middle of the day for Saint Louis. On the 3rd, Saint Denis station did not record any presence of SO_2 while Cambaie station had a gradual increase with a peak of 85 $\mu g\ m^{-3}$ for ORA observation and 135 $\mu g\ m^{-3}$ in MesoNH simulation. Saint Louis has experienced a significant increase with a SO_2 surface concentration of 480 $\mu g\ m^{-3}$ measured by ORA and of 605 $\mu g\ m^{-3}$ simulated by MesoNH, once again in the middle of the day. The 4th of April, no changes occured for Saint Denis, while a strong SO_2 increase appears at Cambaie with 500 $\mu g\ m^{-3}$ in MesoNH and 601 $\mu g\ m^{-3}$ for ORA observations. The same behaviour is also seen for Saint Louis station, with 585 $\mu g\ m^{-3}$ observed against a strong over concentration simulated value of 1135 $\mu g\ m^{-3}$. It is important to note that this latter station is positioned on a very strong gradient of SO_2 (1135 $\mu g\ m^{-3}$ to 220 $\mu g\ m^{-3}$ at 5km away). This strong increase is immediately followed by a sharp decrease at the end of the day, with value below 150 $\mu g\ m^{-3}$ for Cambaie and 200 $\mu g\ m^{-3}$ for Saint Louis. On the 5th SO_2, concentration varies between 30 to 200 $\mu g\ m^{-3}$ for Cambaie, and 10 to 300 $\mu g\ m^{-3}$ for Saint Louis except in the evening (18 UTC) where the simulation does not succeed to keep low concentration values (550 $\mu g\ m^{-3}$ simulated instead of 35 $\mu g\ m^{-3}$ observed). For the simulation's last day, the SO_2 surface concentration given by the model is stronger than observations, with highest values of more than 450 $\mu g\ m^{-3}$ (against 45 $\mu g\ m^{-3}$ observed) at Cambaie and a peak of 590 $\mu g\ m^{-3}$ at Saint Louis instead of 55 $\mu g\ m^{-3}$. The same anomaly appears for Saint Denis, when shortly after 00 UTC , the simulation gives a peak of 450 $\mu g\ m^{-3}$ instead of a total absence of volcanic SO_2 highlighted by ORA measurements. Despite these orders of magnitude anomalies from the April 6th, and the global over exposition of SO_2 surface concentration for Saint Louis, SO_2 concentrations between 2 and April 7 are generally consistent with ORA measurements. The simulation succeed to recreate the paradoxical situation between the highest surface SO_2 concentration measured by ORA the 4 April whereas the paroxysmal intensity of the eruption is in the night (from 20 UTC) of the 5 April and on April 6th.

4.4. Vertical transport above the eruption

The increased lava flow and its greater surface coverage between April 2 and 7 consequently involves an increase in heat flux over the lava flow. Heat flow for the first three days are moderate with an average of 12800 W m^{-2}. Local circulation is still dominated by trade winds with surface winds around 5 m s^{-1}. The plume reached 2.5km ASL. (under 100 $\mu g\ m^{-3}$) and the highest SO_2 concentration value are close to the surface (23000 $\mu g\ m^{-3}$). However, from April 5th, the general trend is the increasing of trade winds (11 m s^{-1} around the eruption zone). This increase induces more heat flux (22500 W m^{-2} April 5) and a local breeze in the eruption area which creates a more efficient vertical transport of volcanic sulfur.

The surface warming and the heat flow associated with the lava flow generate atmospheric instability in the low layers of the troposphere. On Figure 8, the strong convection above the lava flow creates a large mixing area with a maximal negative vertical gradient of equivalent potential temperature of $\partial\theta e/\partial z$ = -1.5K/km between the lava and 7km ASL. Under the influence of the trade winds, the vertical structure of the plume in altitude is moving slightly westward. The vertical wind above the eruption reached 14 m s^{-1} from 3 to 5km ASL. and transports SO_2 up to 8 km high (under 100 $\mu g\ m^{-3}$), ie above the inversion zone trade winds situated between 2.5 and 3.5 km of altitude. At this altitude the plume is in thermodynamic equilibrium with the environment and oriented according to the wind direction, ie west/southwest. The plume is no longer transported to the west, but in the direction of Mauritius and Australia. High values of SO_2 concentration are modeled up to 6km (above 30000 $\mu g\ m^{-3}$) the 6 April (Figure 9, cross section in left panel corresponds to blue line (2 April) in Figure 1 and cross section in right panel corresponds to red line (6 April)).

4.5. Rainfall and aqueous chemistry

The 5 and the 6 April, strong clouds formations appears in the Piton de la Fournaise area. The associated accumulated rainfall simulated between 2 and 7 April 2007 by MesoNH is consistent with Meteo-France observations (Figure 10). Only the southeast weather station gives high rainfall value (67mm cumulated), whereas the western weather station recorded lower value (15mm and 6mm). One possible causes of concentrations overprediction for April 6th is that the scavenging of SO_2 by rain and cloud water leading to sulfuric acid formation is not taken into account in the simulation. However, Meteo-France measurements have shown that between April 2 and 7, the largest quantity of rain were observed only for the 6 April in the volcanic region. As MesoNH includes a cloud chemistry module [*Leriche et al.*, 2013] a sensitivity test was realized from April 5 18 UTC to April 7 00 UTC (limited period due to high computational cost) by activating this module. A simplified mechanism in aqueous phase was used including the oxidation of SO_2 into sulfuric acid by hydrogen peroxide, ozone and pernitric acid [*Leriche et al.*, 2003]. The module includes also the mass transfer kinetic for the exchange between the gas phase and liquid phases of soluble gases and their redistribution between cloud water and rainwater by microphysical processes (collision/coalescence leading to precipitation and sedimentation of raindrops leading to wet deposition).

One of the main consequence of cloud chemistry activation is a global decrease of SO_2 surface concentration due to SO_2 scavenging by rainfall and aqueous phase SO_2 chemistry transformation inside clouds over Reunion Island. The 6 April at 13 UTC, the difference of SO_2 surface concentration between the simulation with cloud chemistry activated (AQ simulation) and reference simulation (REF) reach up to -700 $\mu g\ m^{-3}$ over the high terrain in the center of the island (Figure 11). The SO_2 surface concentration for the western coastline is 200 $\mu g\ m^{-3}$ lower for the AQ simulation than the REF simulation and for the Piton de la Fournaise area, a strong decrease appears due to the proximity of the vent with the presence of high rainfall this day over the volcano. Generally, a 30% to 60% decrease is simulated by MesoNH, giving SO_2 surface concentrations close to ORA observations (Figure 12).

5. Influence of sensible heat fluxes in the transport of SO_2

A sensitivity study was performed to characterize the influence of heat flux forcings over the vent and lava on the vertical transport of SO_2 (Figure 9). To do so, an additional simulation has been made without thermodynamic flux (NO-FLX) to highlight the contribution of these fluxes in the transport and the dispersion of sulfur dioxide. This simulation rapidly presents large discrepancy from the reference simulation (REF) as shown by Figure 13 in the differences of SO_2 concentration (in $\mu g\ m^{-3}$) between the NO-FLX simulation and the REF simulation on the 3,4,5 and 6 of April at 13 UTC. A strong positive difference in concentrations appears for the whole southern part of the island with a maximum of 32000 $\mu g\ m^{-3}$. The northwestern part of the island is also overexposed to higher concentrations of the order of 500 $\mu g\ m^{-3}$ for April 3 and 1000 $\mu g\ m^{-3}$ from April 3 to 5. Conversely, negative anomalies are simulated the 4th of April for the northwest with less than 340 $\mu g\ m^{-3}$ compared to concentrations in the REF simulation. As a main consequence, concentrations obtained with the simulation NO-FLX are also far from ORA measurements. In general, unrealistic peaks are simulated (Figure 14) with a factor of 5 to 35 in the south, and 5 to 10 in the northwest compared to ORA observations. Taking into account sensible heat flux from lava is therefore of prime importance as the NO-FLX simulation did not recreate correctly the spatial and temporal distribution of sulfur dioxide for the 2007 eruption of Piton de la Fournaise. Here, the lack of heat flux injection did not allow adequate vertical transport, essential to get an overall good representation of SO_2 distribution. As a general consequence we estimate that numerical modeling of the April 2007 eruption cannot be represented without heat flux correctly estimated and injected at the eruptive vent.

6. Conclusions

The objective of this study was to model fine scale spatial distribution of SO_2 degassed during the eruption of the Piton de la Fournaise in April 2007. It was necessary to adequately modeled the heat flux injection over the vent and lava flow to simulate the atmosphere dynamics that drives this SO_2 distribution. The simulation has been found to be in relatively good agreement with observations, and highlighted two phases. With moderate value of heat fluxes from lava flow (12800 $W.m^{-2}$), the first phase, between April 2 and 4, shows a SO_2 plume still contained under the trade wind inversion at 3km ASL. The main consequence is a high SO_2 surface concentration for western stations (600 $\mu g\ m^{-3}$ for ORA observations, 500 $\mu g\ m^{-3}$ for simulation at Cambaie). The second phase, between April 5 and 7, corresponds to the eruption maximum intensity. This high intensity is accompanied by a strong increase in lava heat flux (22500 $\mathrm{W\ m^{-2}}$) that allows the SO_2 plume to cross the trade wind inversion, and reach an altitude of 8km ASL on the 6th of April. This deep convection reduces surface SO_2 concentration (600 $\mu g\ m^{-3}$ to 100 $\mu g\ m^{-3}$ in few hours at Cambaie), but the model fails to keep low SO_2 surface concentration on the last simulation day (peaks at 400 $\mu g\ m^{-3}$ instead of 55 $\mu g\ m^{-3}$ at the end of 6 April). These over predictions were addressed by taking into account the cloud chemistry in a sensitivity study realized from 12 UTC on April 5 to April 7. During this period, the scavenging of SO_2 by rain water and cloud water significantly reduces SO_2 surface concentration, producing sulfuric acid and as a consequence acid rain. Overall, the reference simulation was largely in good agreement and within the same order of magnitude, with the observation values from ORA. To highlight heat flux influence, a second sensitivity study was performed, in which the heat fluxes from the vent and lava flow were totally suppressed. Without these additional contributions of heat flux, the simulated surface concentrations are up to 45 times higher than the observations. One of the main conclusions of the study is that heat flux above lava is a crucial parameter to take into account in order to reproduce correctly SO_2 distribution. This additional energy allows the development of strong convection that injects volcanic discharges over the atmospheric boundary layer. The heat flux model, although still imperfect by its surface representation, significantly improve the SO_2 spatial distribution, as shown in this study by respecting orders of magnitude compared to observations and by displaying correct temporal evolution of the simulated surface concentrations.

A perspective of improvement is the implementation of a new deep convection scheme to improve the representation of sub-grid convective transport in MesoNH model. The initial deep convection scheme from MESO-NH basic package is not adapted for an extreme event such as volcanic eruption. Indeed, some important processes are not taken into account or are not representative of a phenomenology of an eruption, such as the speed of ejection of gas and heat flow, or the absence of the mixing vertical processes. A strategy could be a coupling system between a more detailed lava surface model and MesoNH atmospheric model to better reproduce the distribution and evolution of the lava during the period.

Acknowledgments. We greatly acknowledge the MesoNH assistance, especially C.Lac and J.Escobar. Computer resources were provided by CINES (Centre Informatique National de l'Enseignement Supérieur http://www.cines.fr/, project no. lac6309) and CCUR (Centre de Calcul de l'Université de la Réunion) for the access to super-computer. We also thank ORA (http://www.atmo-reunion.net/) for free access to their data. Finally, we would like to thank OSU-R, OMNCG federation, Reunion University and LEFE/INSU program for funding this work.

References

Albrecht, B. A. (1989), Aerosols, cloud microphysics, and fractional cloudiness., *Science*, *245*.

Allen, A. G., P. J. Baxter, and C. J. Ottley (2000), Gas and particle emissions from soufrière hills volcano, montserrat, west indies: characterization and health hazard assessment., *Bull. Volcanol.*, *62*.

Bachèlery, P., F. Saint-Ange, N. Villeneuve, B. Savoye, A. Normand, E. Le Drezen, A. Barrère, J. Quod, and C. Deplus (2014), Aâa lava flows into the sea, april 2007, piton de la fournaise volcano, la réunion island, *Active Volcanoes of the Southwest Indian Ocean: Piton de la Fournaise and Karthala. Active Volcanoes of the World. Springer-Verlag Berlin and Heidelberg*.

Barde-Cabusson, A., S. andÂ Finizola, A. Peltier, M. Chaput, N. Taquet, S. Dumont, Z. Duputel, A. Guy, L. Mathieu, S. Saumet, F. Sorbadère, and M. Vieille (2011), Structural control of collapse events inferred by self-potential mapping on the piton de la fournaise volcano (la reunion island)., *J. Volcanol. Geotherm. Res.*, doi:doi: 10.1016/j.jvolgeores.

Barthe, C., J. Pinty, and C. Mari (2007), Lightning-produced nox in an explicit electrical scheme tested in a stratosphere-troposphere experiment: Radiation, aerosols, and ozone case study, *J.*

Geophys. Res., *112*, doi:10.1029/2006JD007402.

Baxter, P. J., R. Stoiber, and S. N. Williams (1982), Volcanic gases and health: Masaya volcano, nicaragua, *Lancet*, *2*.

Bechtold, P., E. Bazile, F. Guichard, P. Mascart, and E. Richard (2001), A mass-flux convection scheme for regional and global models, *Quart. J. Roy. Meteorol. Soc.*, *127*, 869–886.

Bougeault, P., and P. Lacarrere (1989), Parametrization of orography induced turbulence in a meso-beta model, *Mon. Weather Rev.*, *117*.

Cohard, J., and J. Pinty (2000), A comprehensive two-moment warm microphysical bulk scheme, ii: 2d experiments with a non hysrostatic model, *Q. J. Roy. Meteorol. Soc.*, *126*.

Coppola, D., D. Piscopo, T. Staudacher, and C. Cigolini (2009), Lava discharge rate and effusive pattern at piton de la fournaise from modis data, *J. Volcanol. Geotherm. Res.*, *184*.

Crassier, V., K. Suhre, P. Tulet, and R. Rosset (2009), Development of a reduced chemical scheme for use in mesoscale meteorological models, *Atmos. Environ.*, *34*.

Delmelle, P., J. Stix, C.-A. Bourque, P. Baxter, J. Garcia-Alvarez, and J. Barquero (2001), Dry deposition and heavy acid loading in the vicinity of masaya volcano, a major sulfur and chlorine source in nicaragua, *Env. Sci. Tech.*, *35*.

Di Muro, A., N. Métrich, D. Vergani, M. Rosi, P. Armienti, T. Fougeroux, E. Deloule, I. Arienzo, and L. Civetta (2014), The shallow plumbing system of piton de la fournaise volcano (la réunion island, indian ocean) revealed by the major 2007 caldera forming eruption, *Journal of Petrology*, *accepted in press*.

Fiocco, G., D. Fua, and G. Visconti (1996), The mount pinatubo eruption â effects on the atmosphere and climate, *Springer- Verlag*.

Grini, A., P. Tulet, and L. Gomes (2006), Dusty weather forecast using the mesonh atmospheric model, *Journal of Geophysical Research*, *111*.

Harris, A., J. Bailey, S. Calvari, and J. Dehn (2005), Heat loss measured at a lava channel and its implication for down-channel cooling and rheology, *Geological Society of America*, *Special paper 396*.

Hobbs, P. V., J.-P. Tuell, H. D.-A., L.-F. Radke, and M.-K. Eltgroth (1982), Particles and gases in the emissions from the 1980-1981 volcanic eruptions of mt. st. helens, *Journal of Geophysical Research*, *87*.

Hoffman, D.-J. (1987), Perturbations to the global atmosphere associated with the el chichon volcanic eruption of 1982, *Rev. Geophys.*, *25*.

Kaufman, Y. J., D. Tanra, and O. Boucher (2000), A satellite view of aerosols in the climate system, *Nature*, *419(6903)*.

Keszthelyi, L., A. Harris, and J. Dehn (2003), Observations of the effect of wind on the cooling of active lava flows., *Journal of Geophysical Research*, *SDE 4-1*.

Klingelhofer, F., M. Hort, H.-J. Kumpel, and H.-U. Schemincke (1999), Constraints on the formation of submarine lava flows from numerical model calculations., *Journal of Volcanological and Geothermal Research*, *92*.

Lafore, J., J. Stein, N. Asencio, P. Bougeault, V. Ducrocq, J. Duron, C. Fischer, P. Hereil, P. Mascart, V. M. J. Pinty, J. Redelsperger, E. Richard, and J. V.-G. de Arellano (1998), The meso-nh atmospheric simulation system. part i: adiabatic formulation and control simulations, *ang*, *16*, 90–109.

Leriche, M., D. Voisin, N. Chaumerliac, A. Monod, and B. Aumont (2000), A model for tropospheric multiphase chemistry: application to one cloudy event during the cime experiment, *Atmos. Environ.*, *34*, 5015–5036.

Leriche, M., L. Deguillaume, and N. Chaumerliac (2003), Modeling study of strong acids formation and partitioning in a polluted cloud during wintertime, *Journal of Geophysical Research*, *108*, doi:10.1029/2002JD002950.

Leriche, M., J. Pinty, C. Mari, and D. Gazen (2013), A cloud chemistry module for the 3-d cloud-resolving mesoscale model meso-nh with application to idealized cases, *Geosci. Model Dev.*, *6*, 1275–1298.

Mannino, D., S. Ruben, F. Holschuh, T. Holschuh, M. Wilson, and T. Holschuh (1996), Emergency department visits and hospitalizations for respiratory disease on the island of hawaii, *Hawaii Med. J.*, *55*.

Masson, V. (2000), A physically-based scheme for the urban energy balance in atmospheric models, *blm*, *94*, 357–397.

McCornick, M.-P., L.-W. Thomason, and C.-R. Trepte (1995), Atmospheric effects of the mt pinatubo eruption, *Nature*, *373*.

Michon, L., T. Staudacher, V. Ferrazzini, P. Bachelery, and J. Marti (2007), April 2007 collapse of piton de la fournaise: a new example of caldera formation, *Geophys. Res. Lett.*, *31*, doi:10.1029/2007GL031248.

Michon, L., A. Di Muro, N. Villeneuve, C. Saint-Marc, P. Fadda, and F. Manta (2013), Explosive activity of the summit cone of piton de la fournaise volcano (la réunion island): a historical and geological review, *J. Volcanol. Geotherm. Res.*, *263*, doi:10.1016/J.jvolgeores.2013.06.012.

Mokhtari, M., L. Gomes, P. Tulet, and T. Rezoug (2012), Importance of the surface size distribution of erodible material: an improvement on the dust entrainment and deposition (dead) model, *Geosci. Model Dev.*, *5*, doi:10.5194/gmd-5-581.

Noilhan, J., and J. Mahfouf (1996), The isba land surface parameterization scheme., *Global and Plan. Change*, *13*, 145–159.

Oppenheimer, C. (1991), Lava flow cooling estimated from landsat thematic mapper infrared data: the lonquimay eruption (chile, 1989)., *Journal of Geophysical Research*, *96*.

Oppenheimer, C. (2003), Climatic, environmental and human consequences of the largest known historic eruption: Tambora volcano (indonesia) 1815, *Progress in Physical Geography*, *27*.

Pergaud, J., V. Masson, S. Malardel, and F. Couvreux (2009), A parameterization of dry thermals and shallow cumuli for mesoscale numerical weather prediction, *Boundary-Layer Meteorology*, *132*.

Pollack, J.-B., O.-B. Toon, E.-F. Danielsen, H. D.-J., and J.-M. Rosen (1983), The el chichon volcanic cloud - an introduction, *Geophys. Res. lett.*, *10*.

Quareni, F., A. Tallarico, and M. Dragoni (2004), Modeling of the steady state temperature field in lava flow levees., *Journal of Volcanological and Geothermal Research*, *132*.

Robock, A. (2000), Volcanic eruptions and climate, *Rev. Geophys.*, *38*.

Robock, A. (2002), Pinatubo eruption - the climatic aftermath., *Science*, *295*.

Roult, G., A. Peltier, B. Taisne, T. Staudacher, V. Ferrazzini, A. Di Muro, and O. team (2012), A new comprehensive classification of the piton de la fournaise activity spanning the 1985â2010 period. search and analysis of short-term precursors from a broad-band seismological station, *JVGR*, doi:10.1016/j.jvolgeores.2012.06.012.

Salgado, R., and P. Le Moigne (2010), Coupling of the flake model to the surfex externalized surface model., *Boreal Env. Res.*, *15*.

Solomon, S. (1999), Stratospheric ozone depletion: A review of concepts and history., *Rev. Geophys.*, *37*.

Staudacher, T., V. Ferrazzini, A. Peltier, P. Kowalski, P. Boissier, and al (2009), The april 2007 eruption and the dolomieu crater collapse, two major events at piton de la fournaise (la reunion island, indian ocean)., *Journal of Volcanology and Geothermal Research*.

Suhre, K., C. Mari, T. Bates, J. Johnson, R. Rosset, Q. Wang, A. Bandy, D. Blake, S. Businger, F. Eisels, B. Huebert, G. Kok, R. Mauldin, A. Prevot, R. Schillawski, D. Tanner, and D. Thornton (1998), Physico-chemical modeling of the first aerosol characterization experiment (ace 1) lagrangian b, 1. a moving column approach., *Journal of Geophysical Research*, *103*.

Tulet, P., and N. Villeneuve (2010), Large scale modeling of the transport, the chemical transformation and the mass budget of the sulfur emitted during the eruption of april 2007 by the piton de la fournaise., *Atmos. Chem. Phys. Discuss.*, *10*, doi:10.5194/acpd-10-21357-2010.

Tulet, P., V. Crassier, F. Solmon, D. Guedalia, and R. Rosset (2003), Description of the mesoscale nonhydrostatic chemistry model and application to a transboundary pollution episode between northern france and southern england., *Journal of Geophysical Research*, *108*, doi:10.1029/2000JD000301.

Tulet, P., V. Crassier, F. Cousin, K. Suhre, and R. Rosset (2005), Orilam, a three moment lognormal aerosol scheme for mesoscale atmospheric model, on-line coupling into the mesonh-c model and validation on the escompte campaign., *Journal of Geophysical Research*, *110*, doi:10.1029/2004JD005716.

Vlastélic, I., G. Menard, M. Gannoun, J.-L. Piro, T. Staudacher, and V. Famin (2012), Magma degassing during the april 2007 collapse of piton de la fournaise: The record of semi-volatile trace elements, *Journal of Volcanology and Geothermal Research*, *256*.

Yuan, T., L. Remer, and H. Yu (2011a), Microphysical, macrophysical, and radiative signatures of volcanic aerosols in trade wind cumulus observed by the a-train, *Atmos.Chem.Phys*, *11*, 7119–7132, doi:0.5194/acp-11-7119-2011.

Yuan, T., L. Remer, K. Pickering, and H. Yu (2011b), Observational evidence of aerosol enhancement of lightning activity and convective invigoration, *Geophys.Res.Lett.*, *38*, doi: 1029/2010/GL046052.

Simulation	Period	Lava heat flux	Cloud chemistry
REF	04/02 00 UTC - 04/07 00 UTC	Yes	No
NO-FLX	04/02 00 UTC - 04/07 00 UTC	No	No
AQ	04/05 18 UTC - 04/07 00 UTC	Yes	Yes

Table 1. The 3 simulations configurations. REF is the reference simulation, NO-FLX is the simulation without heat fluxes from lava flows and AQ is the simulation with cloud chemistry activated

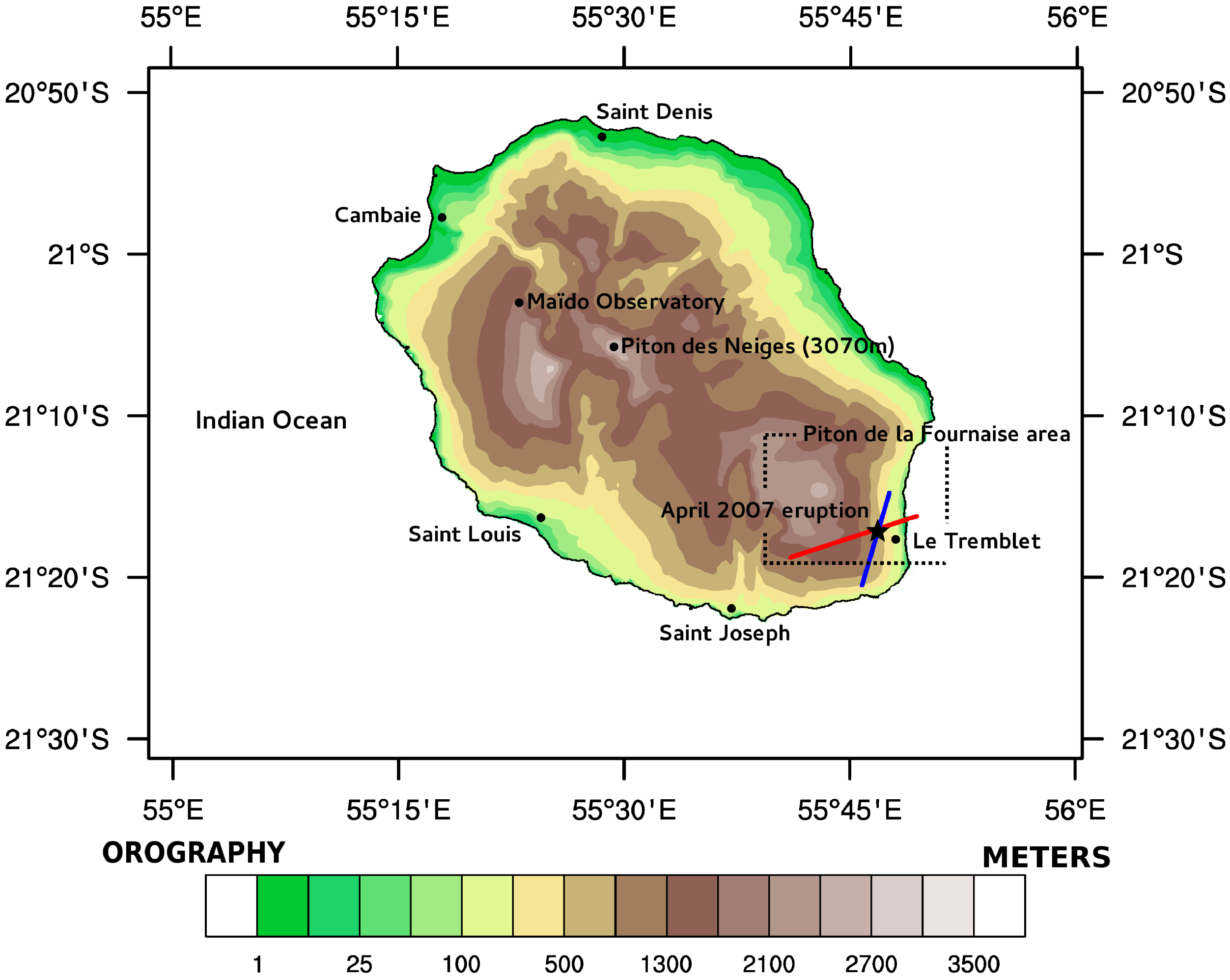

Figure 1. Orography and geographic situation of Reunion Island. The blue line and the red line in the Piton de la Fournaise area correspond respectively to the cross section of 2 April 2007 and 6 April 2007 describes in section 4-3.

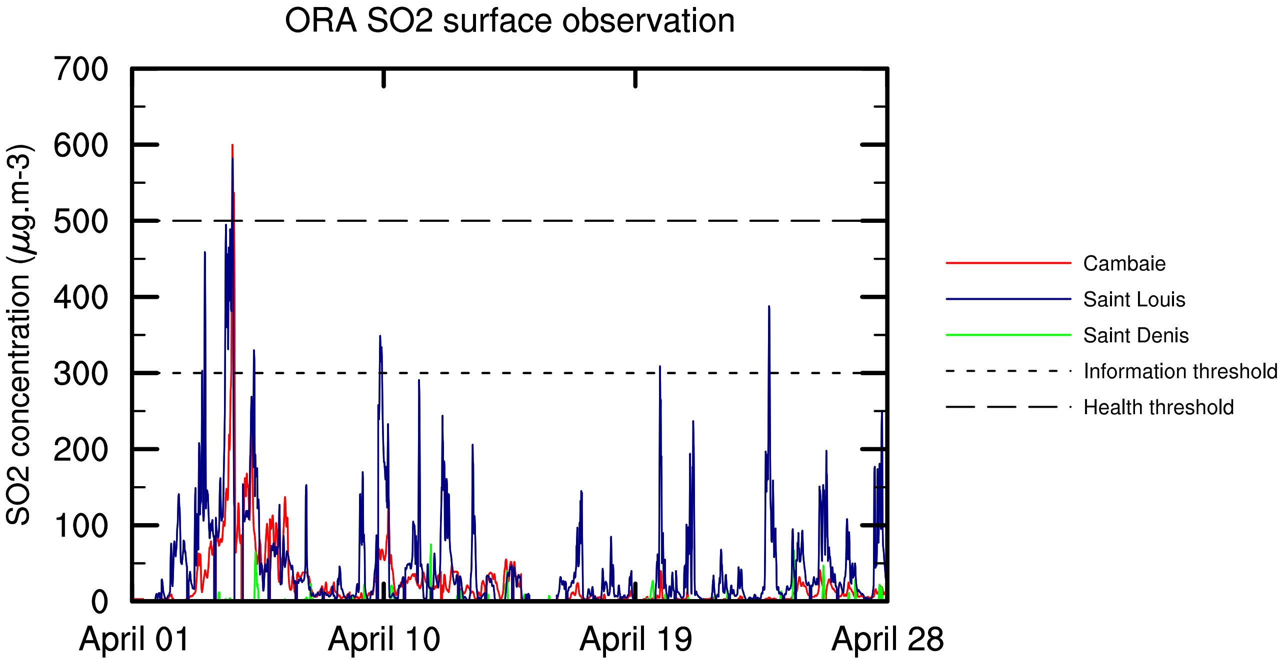

Figure 2. ORA measurements between April 1st and April 28th for Cambaie in the northwest (red), Saint Louis in the southwest (blue) and Saint Denis in the north (Green). Thin dashed line is the public information threshold and the large dashed line is the health threshold.

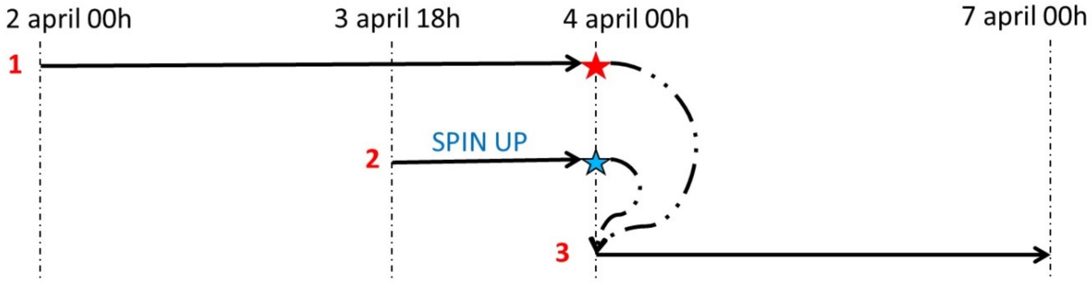

Figure 3. Updating the model dynamic: As a first step, the reference simulation begins the 2 April until 4 April 00 UTC (1). Then a new simulation begins April 3 18 UTC until 4 April 00 UTC (2). This latter will give the new model dynamics while avoiding the early simulation spin up. Finally, the REF simulation resumes the 4 April 00 UTC into the end, with chemical fields of (1) and model dynamic of (2).

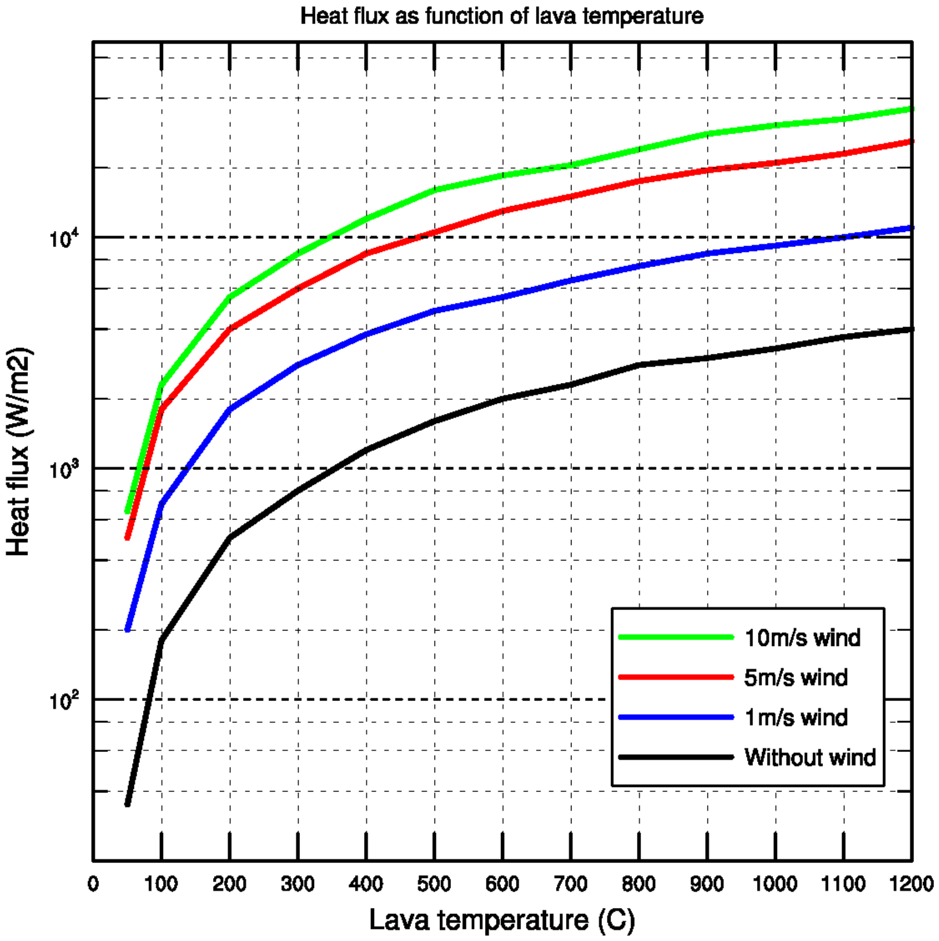

Figure 4. Heat flux evolution with lava surface temperature (Kezsthelyi et al, 2003). The green, red, blue and black lines represent heat fluxes respectively for 10 m s^{-1}, 5 m s^{-1}, 1 m s^{-1} and without surface wind.

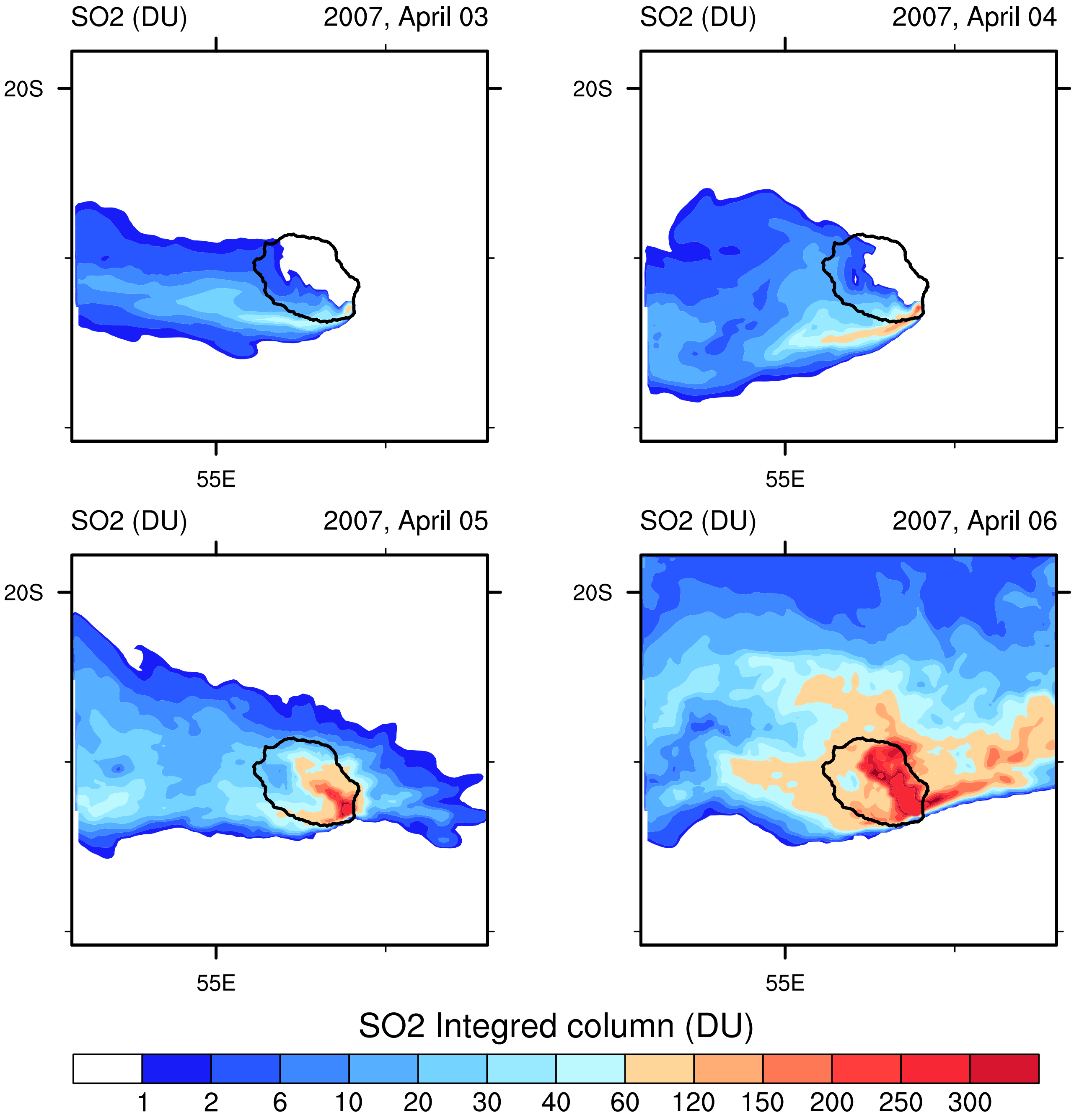

Figure 5. Integred column of SO_2 (DU) between April 3 and April 6 at 13 UTC above the Reunion Island from first model domain (2km horizontal model grid spacing). April 2 and 3 , the SO_2 plume, influenced by the trade winds below the thermic inversion, is oriented to the west. The 4 and 5 April, a large part of the SO_2 plume are crossing the trade winds inversion and is transported to the northeast.

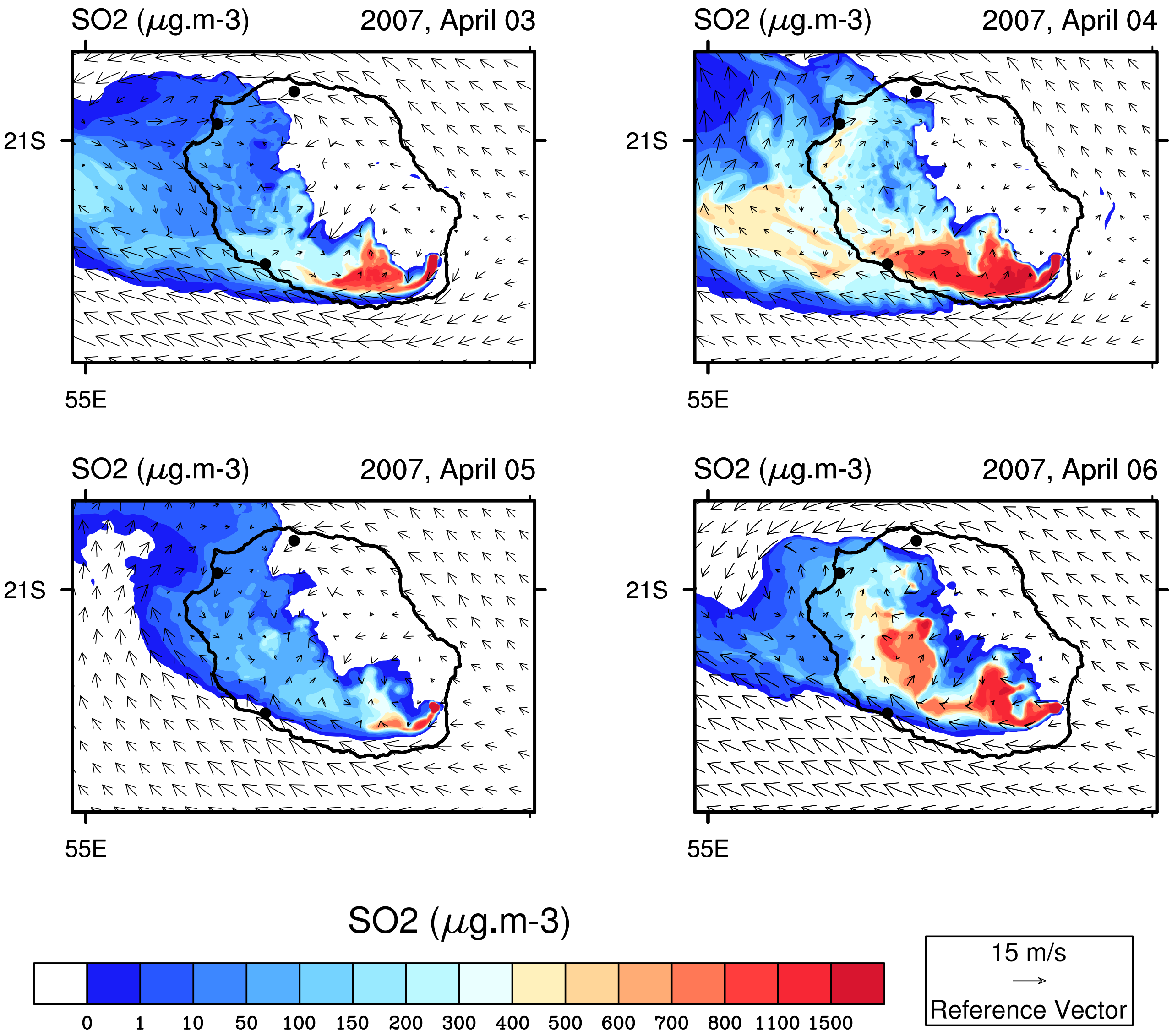

Figure 6. Surface concentration of SO_2 between April 3 and 6 at 13 UTC from MesoNH mesoscale atmospheric model smallest domain (500m horizontal model grid spacing)

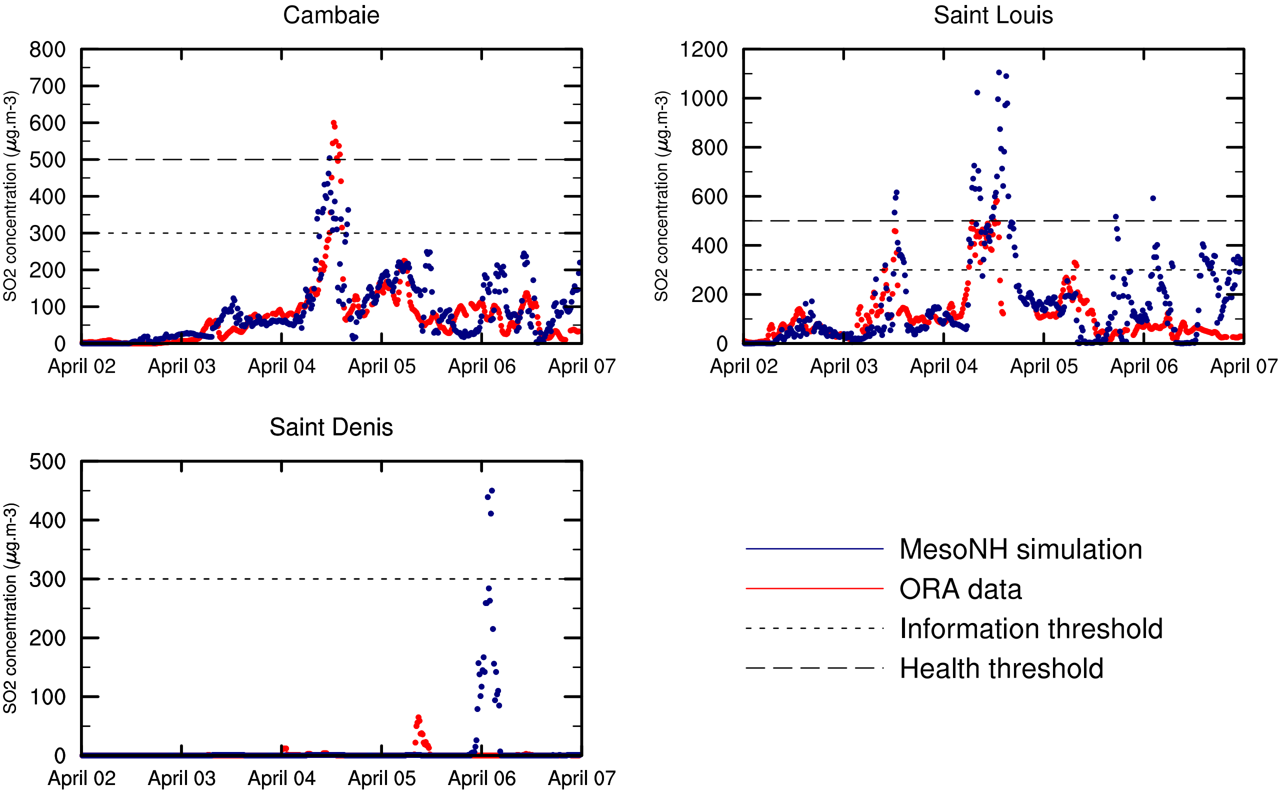

Figure 7. Comparison between ORA observation (blue points) and MesoNH simulation (red points) from April 2 to 7 April. The large dashed line is the health threshold while the thin dashed line is the information threshold.

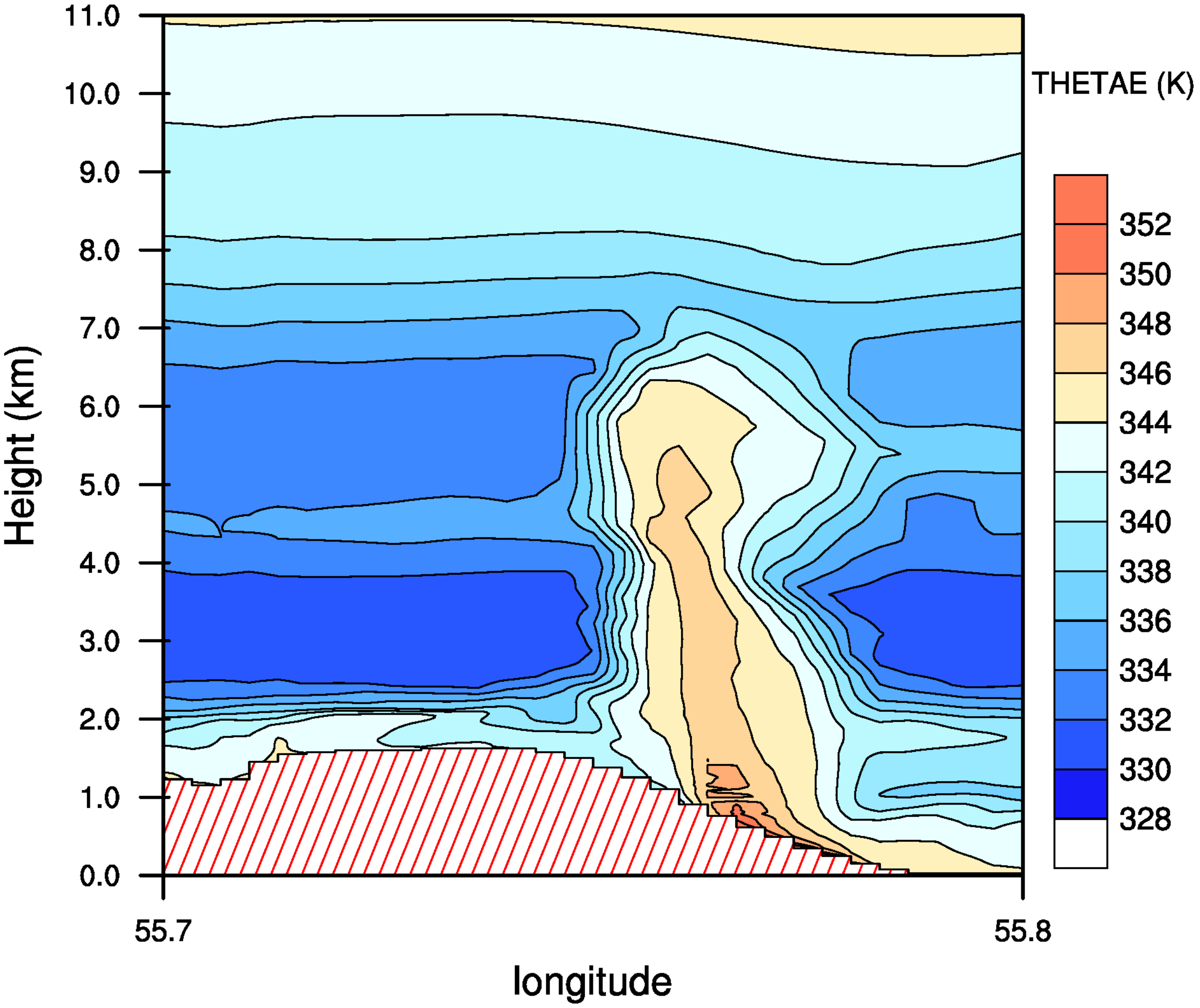

Figure 8. Cross section of equivalent potential temperature (K) for the 6th April at 13 UTC along red line in Figure 1. The strong convection above the lava flow creates a large mixing area with a maximal negative vertical gradient of equivalent potential temperature of $\partial\theta e/\partial z$ = -1.5K/km between the lava and 7km ASL. Under the influence of the trade winds, the vertical structure of the plume in altitude is moving slightly westward.

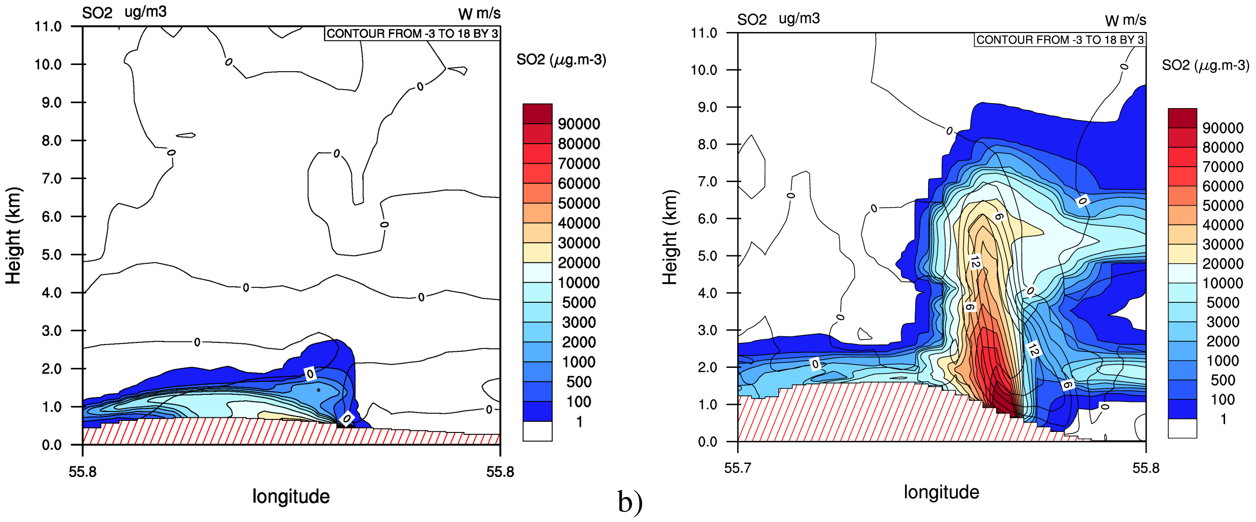

a) b)

Figure 9. Cross section along SO_2 plumes for April 3 (left) and April 6 (right) at 13 UTC. The cross sections are not in the same direction due to change of plume orientation. The left panel corresponds to blue line in Figure 1, the right panel to red line. Color filling corresponds to SO_2 concentrations ($\mu g\ m^{-3}$), isocontours values represent the upward velocity intensity (m s^{-1}) generated by lava heat flow.

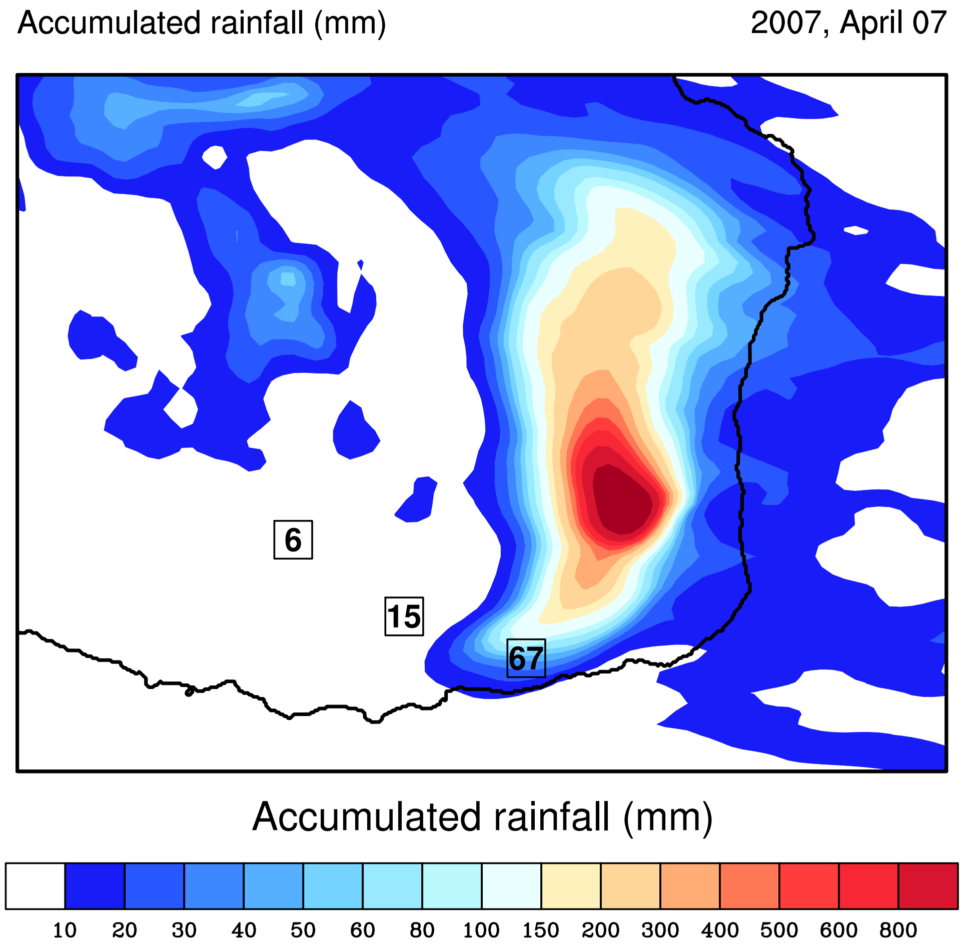

Figure 10. Accumulated rainfall given by MesoNH model between 2 and 7 April 2007. The numbers correspond to Meteo-France observations.

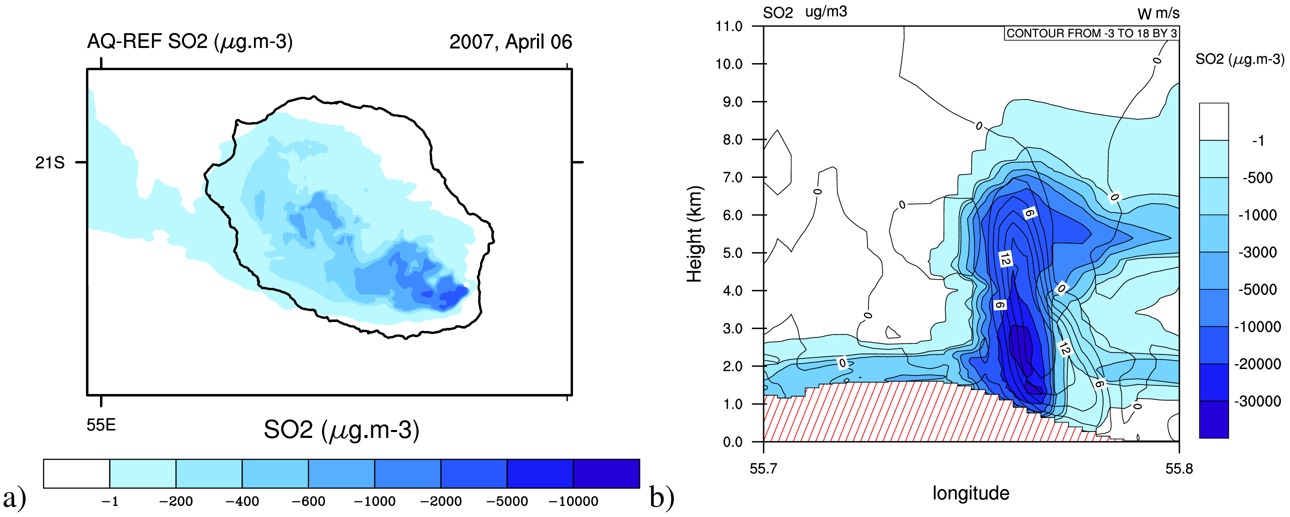

Figure 11. Difference of SO_2 concentration between AQ and REF simulation the 6 April at 13 UTC at the surface (left panel) and in the plume (right panel).

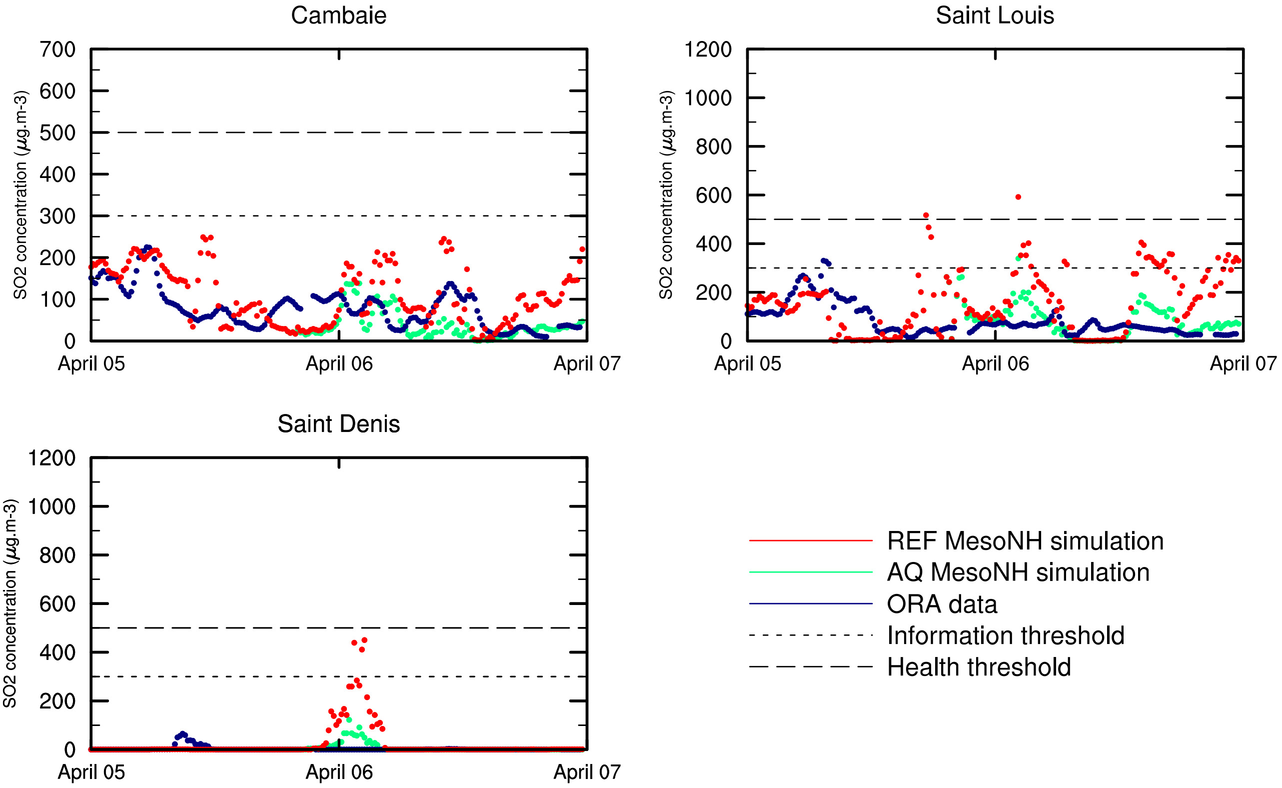

Figure 12. Comparison surface SO_2 concentration between between REF simulation and AQ simulation with observation providing by ORA.

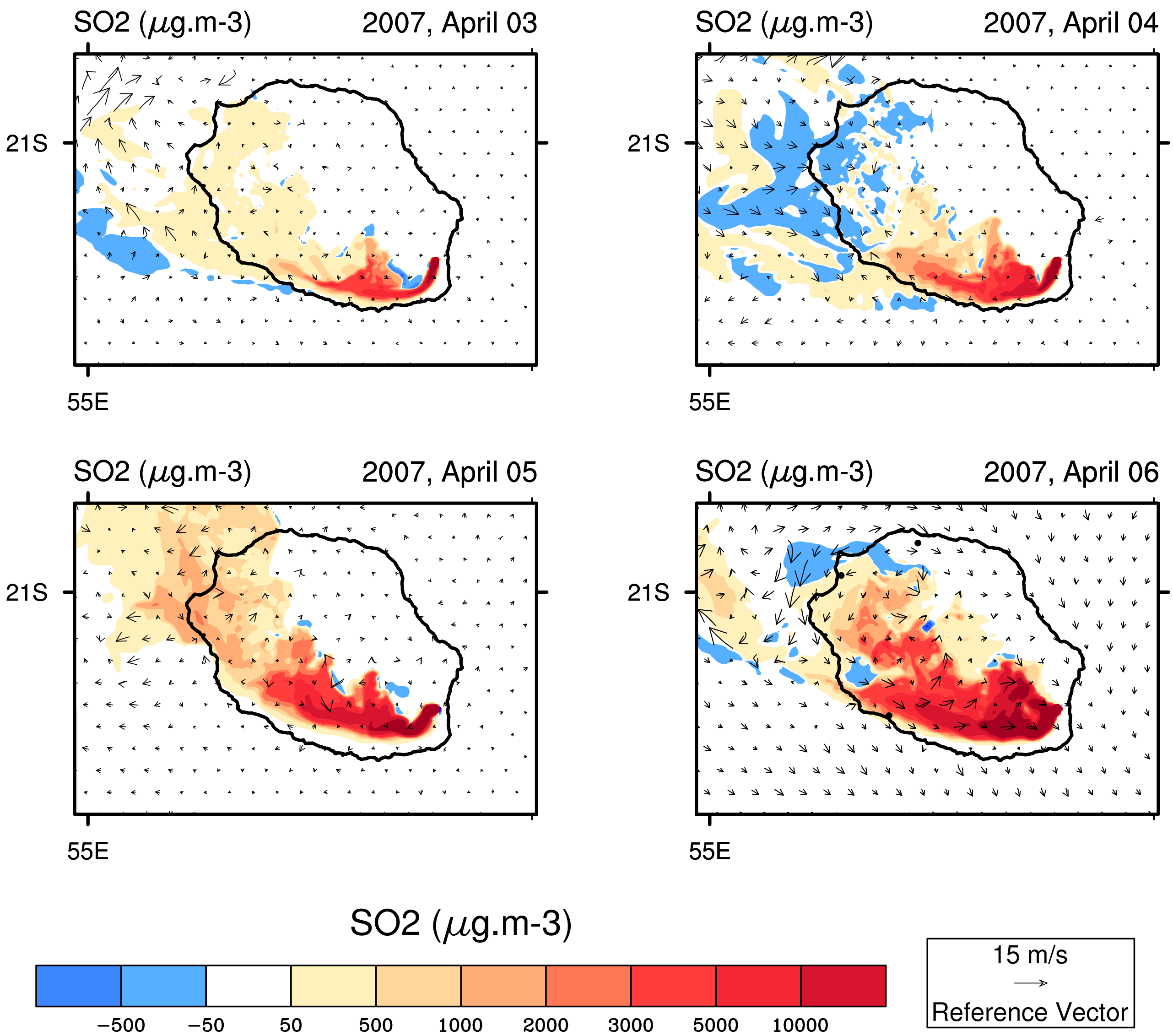

Figure 13. SO_2 concentration difference at the surface between NO-FLX and REF simulations, for April 3,4,5 and 6 2007 at 13 UTC. The arrows represent the difference of the wind field between NO-FLX simulation and REF simulation.

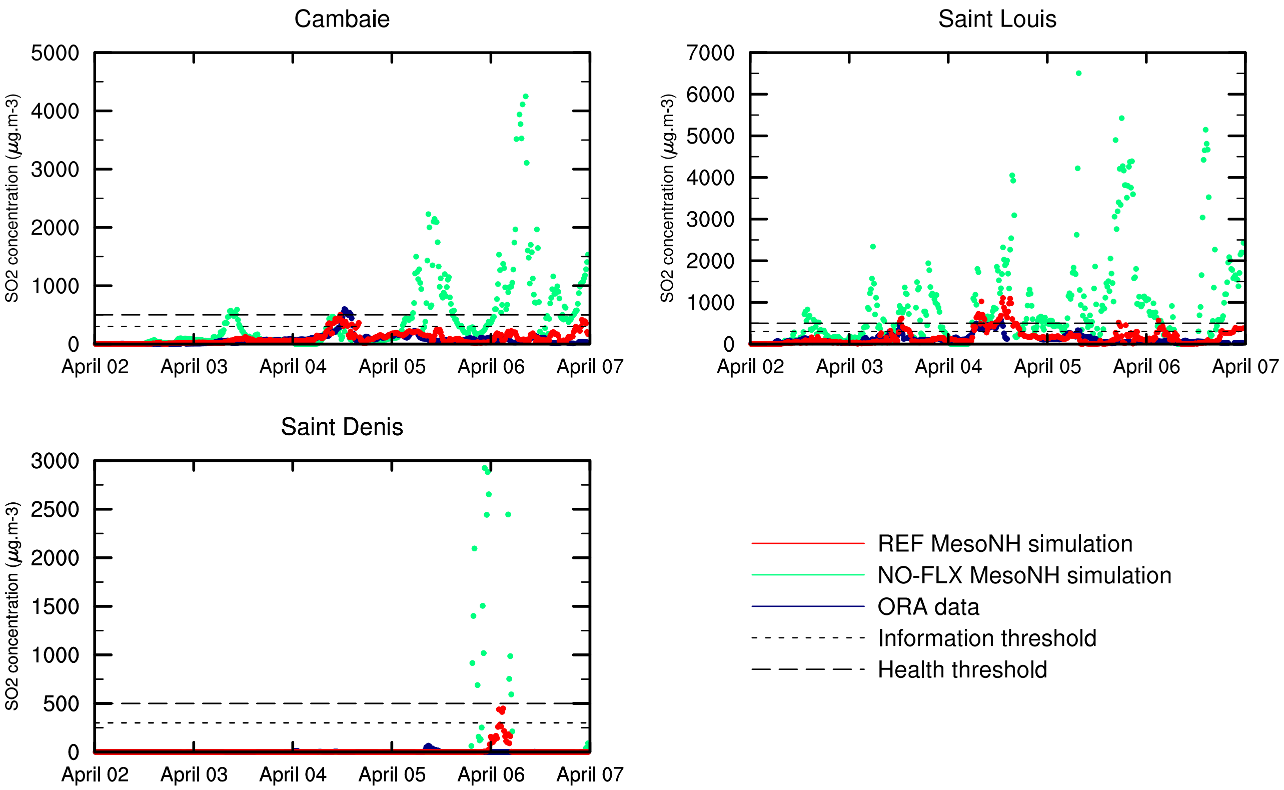

Figure 14. Comparison of surface SO_2 concentration between NO-FLX simulation (green), REF simulation (red) and ORA measurements (blue). Thin dashed line is the public information threshold. Large dashed line is the health threshold.